

TERMINAL GUIDANCE USING A DOPPLER BEAM SHARPENING RADAR

Jeremy A. Hodgson*, BSc(Hons), MSc, MIEE
The MathWorks Ltd,
Cambridge, UK

David W. Lee†, BSc(Hons),MSc
QinetiQ Limited,
Farnborough, UK

Abstract

This paper investigates the guidance issues relating to the use of a form of Synthetic Aperture Radar (SAR) to locate a static target during the terminal phase of an air-to-surface missile engagement. Synthetic Aperture Radars generate “photographic” images of the ground below through the transmission and reception of electromagnetic energy. The clarity of the images will depend on the resolution both along, and perpendicular, to the line of sight between the observer and a point on the ground. The resolution along the line of sight is controlled through the transmitted pulsewidth, and the cross range resolution through the incremental Doppler shift of adjacent points on the ground. This paper focuses on the use of a particular form of SAR known as Doppler Beam Sharpening (DBS) to generate images that can be used to guide a missile onto a target. For a successful engagement the missile must fly a trajectory that satisfies a number of requirements. The generated images must be of sufficiently high resolution that the target can be identified; the information extracted from successive images must be sufficient for the guidance filters to accurately determine the position of the target; and finally, the missile must be able to hit the target at a desired speed, flightpath angle, and with a low angle of attack to achieve a kill. In this paper a trajectory optimization technique is used to shape the trajectory to achieve these requirements, and a candidate guidance law is demonstrated where the gains are determined so that the missile follows the nominal optimal trajectory, and achieves a low miss distance at impact.

1. Introduction

The basis for the use of a DBS radar for generating images is that a lower cross range resolution can be obtained for a given antenna length by making use of the Doppler shift in the frequency of the returned signal due to the relative motion between the target object and the missile. The magnitude of the Doppler shift that can be resolved is a function of the radar illumination time (dwell time). The cross range resolution that can then be achieved is dependent upon both the resolvable Doppler shift, and the offset angle between the velocity vector and the line of sight. In order to image the target the missile must therefore fly with a heading offset

from the line of sight, until a point is reached where imaging will no longer be possible, and the missile will fly towards the best estimate of the target location. A modified form of velocity pursuit guidance for use with a SAR sensor is outlined in Zipfel². The guidance law shapes the trajectory to follow analytical functions (e.g. circular, or spiral shapes) in order to maintain the angular offset, and bring the missile along a desired line of approach at impact. The limitation of this form of guidance law is that it does not account for constraints imposed by limited acceleration capabilities of the missile airframe, or constraints imposed by gimbal limits restricting the maximum look angle between the line of sight and the velocity vector. It is also unable to account for the missile drag characteristics, which is needed to meet requirements on the velocity at impact.

Trajectory optimization methods have been employed in a number of applications^{3,7} to determine nominal trajectories that minimize certain objectives, constrain the control demands, and impose interior point constraints on functions of the states. This paper demonstrates the use of optimization methods to determine trajectories which aim to minimize the dwell time to achieve a desired cross range resolution during the imaging period, satisfy control and look angle constraints, and which meet the flight requirements at impact.

Generating images with the required resolution so that the target object can be identified does not on its own guarantee good guidance loop performance. Measurements of the range to the target, and the Doppler shift at the target location can be extracted from each image. The target position relative to the missile can then be derived using these measurements, and the velocity and height estimates from an Inertial Navigation System (INS). Any errors in the INS estimates will lead to inaccurate estimates of the target location, hence an estimator is required to provide a filtered value of the relative location of the target to the missile, and an estimate of the error in the velocity output from the INS. A comparison of the filter methods that can be applied to this problem is given in Rollason⁸ and Ristic⁴. For this paper the expected accuracy to which the target location can be estimated is quantified by determining the Cramer-Rao Lower Bound (CRLB) at the end of the imaging period. The CRLB is determined for a non-linear least squares batch filter utilizing a stored set of measurements taken at intervals during the engagement. The effect on the optimal trajectories of including the magnitude of the

* Senior Engineer, Consulting

† Team Leader, Guidance and Imaging Solutions

CRLB as a cost to be minimized is investigated in this paper.

Finally, a modified form of the guidance law outlined in Zipfel² is developed which shapes the trajectory to follow the nominal optimal trajectories.

The following Sections include a description of the model to represent the dynamics of the missile; a derivation of the relationship between the DBS cross range resolution, the dwell time, and the missile to target geometry; a derivation of the CRLB for the batch filter; the optimization method employed and the resulting trajectories, and finally the closed loop guidance law and a comparison between the open and closed loop trajectories that are followed.

2. Missile dynamic model

The equations that represent the dynamics of a point mass missile model, in the unrolled coordinate system in Figure 1, are given in Equation (2.1). The states consist of the position of the missile (x, y, h) , the pitch and yaw (γ, ψ) flightpath angles, and the specific energy $\left(E = h + \frac{V^2}{2g}\right)$. At any point the velocity (V) can be derived directly from the algebraic relationship with the specific energy. The control variables are the demanded accelerations (a_y, a_z) applied normal to the velocity vector, and the thrust level (T) , which is assumed to be variable but fixed during the final stages of the engagement.

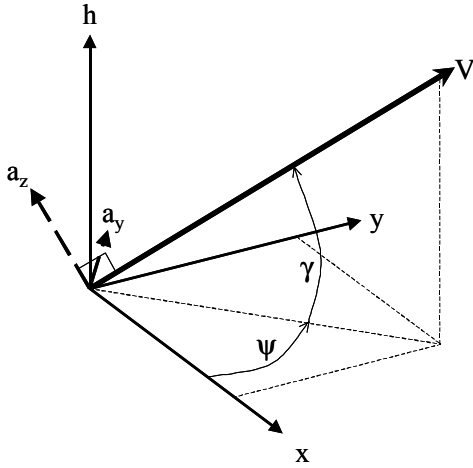


Figure 1: Coordinate System

$$\begin{aligned}\dot{x} &= V \cos \gamma \cos \psi \\ \dot{y} &= V \cos \gamma \sin \psi \\ \dot{h} &= V \sin \gamma \\ \dot{\gamma} &= \frac{(a_z - \cos \gamma) \cdot g}{V} \\ \dot{\psi} &= \frac{a_y \cdot g}{V \cos \gamma} \\ \dot{E} &= \frac{V \cdot (T - D)}{mg}\end{aligned}\quad (2.1)$$

In Equation (2.1), the missile drag (D) is calculated using Equations (2.2) and (2.3), where the drag coefficient (C_D) is a function of the zero incidence drag (C_{D0}) , and the induced drag coefficient (k) .

$$D = \frac{1}{2} \rho V^2 S_{\text{Ref}} C_D \quad (2.2)$$

$$\begin{aligned}\rho &= \rho_0 \left(\frac{T_0 + Lh}{T_0} \right)^{\left(\frac{g}{LR} - 1 \right)} \\ C_D &= C_{D0} + k C_L^2 \\ C_L &= \frac{mg(a_z^2 + a_y^2)^{1/2}}{\frac{1}{2} \rho V^2 S_{\text{Ref}}}\end{aligned}\quad (2.3)$$

An estimate for the total angle of attack (α) can be obtained by assuming an approximately linear relationship with the lift coefficient (C_L) in Equation (2.4).

$$\alpha = \frac{C_L}{C_{L\alpha}} \quad (2.4)$$

Characteristics for a representative air-to-surface missile are given in Farooq⁷, and are presented in Table 1.

3. Determining the achievable cross range resolution

The Doppler shift from a point on the ground can be determined by considering the difference between transmitted and received frequencies when the range to the object is varying. The Doppler shift from point A in Figure 2 is given by Equation (3.1), where $\sigma_v = \cos^{-1}(\underline{\bar{u}}_v \cdot \underline{\bar{u}}_{\text{LOS}})$ is the total angle between the velocity vector and the line of sight, $\underline{\bar{u}}_v$ is a unit vector along the velocity vector, and $\underline{\bar{u}}_{\text{LOS}}$ is a unit vector along the line of sight defined by the pitch and yaw sightline angles in Equation (3.3).

$$f_d|_A = f_{\text{Return}} - f_{\text{Transmitted}} = -\frac{2}{\lambda} \dot{R} = \frac{2}{\lambda} V \cos(\sigma_v) \quad (3.1)$$

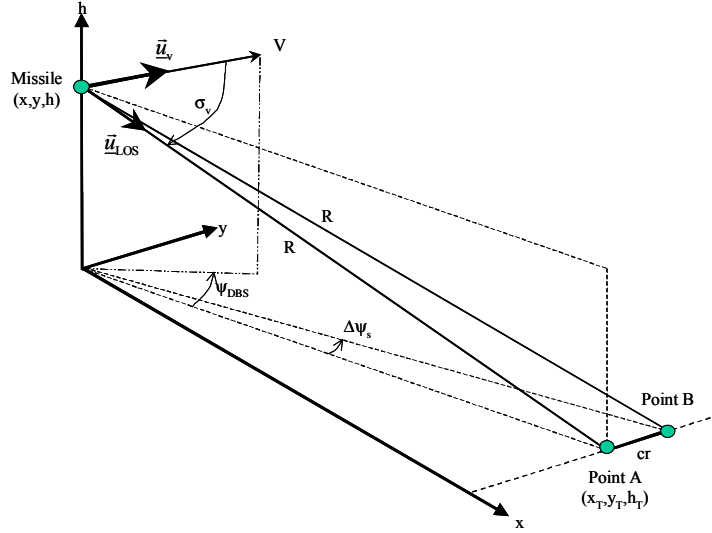


Figure 2: Missile to Target Geometry

$$\vec{u}_v = \begin{bmatrix} c \gamma c \psi \\ c \gamma s \psi \\ s \gamma \end{bmatrix}, \vec{u}_{LOS} = \begin{bmatrix} c \gamma_s c \psi_s \\ c \gamma_s s \psi_s \\ s \gamma_s \end{bmatrix} \quad (3.2)$$

$$(c \gamma = \cos \gamma \text{ \& } s \gamma = \sin \gamma)$$

$$\gamma_s = \tan^{-1} \left(\frac{h_T - h}{\sqrt{(x_T - x)^2 + (y_T - y)^2}} \right) \quad (3.3)$$

$$\psi_s = \tan^{-1} \left(\frac{(y_T - y)}{(x_T - x)} \right)$$

The first step to derive an expression for the achievable cross range resolution is to determine the difference in the Doppler frequency shift between point A, and a point B that is at the same range (R), and a small horizontal rotation ($\Delta \psi_s$) from point A.

The difference in the Doppler shift (Δf) from the 2 points is given by Equation (3.4).

$$\Delta f = \frac{2V}{\lambda} \left(\begin{bmatrix} c \gamma c \psi \\ c \gamma s \psi \\ s \gamma \end{bmatrix} \cdot \begin{bmatrix} c \gamma_s c \psi_s \\ c \gamma_s s \psi_s \\ s \gamma_s \end{bmatrix} - \begin{bmatrix} c \gamma c \psi \\ c \gamma s \psi \\ s \gamma \end{bmatrix} \cdot \begin{bmatrix} c \gamma_s c(\psi_s + \Delta \psi_s) \\ c \gamma_s s(\psi_s + \Delta \psi_s) \\ s \gamma_s \end{bmatrix} \right) \quad (3.4)$$

Expanding out Equation (3.4), and using small angle approximations for $\Delta \psi_s$ gives the expression for Δf in Equation (3.5).

$$\Delta f = -\frac{2V}{\lambda} \cos \gamma \cos \gamma_s \sin(\underbrace{\psi - \psi_s}_{\psi_{DBS}}) \Delta \psi_s \quad (3.5)$$

If the small horizontal angular difference between the sightline to point A and point B is given by (3.6), and the magnitude of the minimum resolvable Doppler frequency shift is given by (3.7), then the relationship

between the dwell time, and the achievable cross range resolution is given by Equation (3.8).

$$\Delta \psi_s = \frac{cr}{(R \cos \gamma_s)} \quad (3.6)$$

$$|\Delta f| = \frac{1}{\text{Dwell Time}} \quad (3.7)$$

$$cr \times \text{Dwell Time} = crDT = \frac{\lambda}{2} \frac{R}{(V \cdot \cos \gamma \cdot \sin \psi_{DBS})} \quad (3.8)$$

For the purposes of this paper it is assumed that $3m^{-1}$ is the recommended resolution cell size to identify vehicles or buildings from an image. It is also assumed that an object can only be seen if the range is less than the acquisition range $R_{Acquire}$ defined by the power of the radar.

4. Determining the uncertainty in the estimate of the target location

The aim of this Section is to derive a measure of the accuracy to which the location of the target can be determined from a discrete number (n_{image}) of images generated at intervals during an engagement when using a non-linear least squares batch filter. A comparison of the performance of the batch filter compared to other estimation methods is given in Rollason⁸. It is assumed in the filter that the true relative positions ($\underline{x}_T - \underline{x}_M$), and velocities ($\underline{v}_T - \underline{v}_M$), are related to the INS estimates ($\underline{x}_{INS}, \underline{v}_{INS}$) by Equation (4.1). In (4.1), the error at a time t from when observations commence is a function of the position errors ($\delta \underline{x}_f$) at the end of the period of observation ($t = t_{f_image}$), and constant velocity errors ($\delta \underline{v}$).

$$\begin{aligned}
(\underline{x}_T - \underline{x}_M)_{True} &= \underline{x}_{INS} + (\underline{\delta x}_f - \underline{\delta v} \times \Delta t) \\
(\underline{v}_T - \underline{v}_M)_{True} &= \underline{v}_{INS} + \underline{\delta v} \\
\text{Where } \Delta t &= t_{f_image} - t \\
\underline{\delta x}_f &= \begin{bmatrix} \delta x \\ \delta y \\ \delta h \end{bmatrix}, \underline{\delta v} = \begin{bmatrix} \delta v_x \\ \delta v_y \\ \delta v_h \end{bmatrix}
\end{aligned} \tag{4.1}$$

The constant parameters $\underline{x} = \begin{bmatrix} \underline{\delta x}_f \\ \underline{\delta v} \end{bmatrix}$ are to be estimated

from a stored set of measurements extracted from the images. The measurements are assumed to be the range to the target, and the range rate derived from the Doppler frequency shift. The measurements are related to the INS estimates, and the unknown parameters, through Equation (4.2).

$$\begin{aligned}
z_R &= h_R(\underline{x}_{INS}, \underline{v}_{INS}, \underline{x}, \Delta t) \\
&= \sqrt{\begin{aligned} &(x_{INS} + \delta x - \delta v_x \Delta t)^2 \\ &+ (y_{INS} + \delta y - \delta v_y \Delta t)^2 \\ &+ (h_{INS} + \delta h - \delta v_h \Delta t)^2 \end{aligned}} \\
z_{\dot{R}} &= h_{\dot{R}}(\underline{x}_{INS}, \underline{v}_{INS}, \underline{x}, \Delta t) \\
&= \frac{(\underline{x}_{INS} + \underline{\delta x}_f - \underline{\delta v} \cdot \Delta t) \cdot (\underline{v}_{INS} + \underline{\delta v})}{z_R}
\end{aligned} \tag{4.2}$$

Each measurement is assumed to be independent, and has zero mean Gaussian uncertainty with a standard deviation given by Equation (4.3).

$$\begin{aligned}
\sigma_R &= R_{Res} \\
\sigma_{\dot{R}} &= \left(\frac{\lambda}{2} \right) \frac{cr}{crDT}
\end{aligned} \tag{4.3}$$

The CRLB provides a lower bound on the achievable variance in the estimation of a parameter. For an unbiased estimator it is given by the inverse of the Fisher Information Matrix (J) in Equation (4.4).

$$E[(\underline{x}_{True} - \hat{\underline{x}})(\underline{x}_{True} - \hat{\underline{x}})^T] \geq J^{-1} \tag{4.4}$$

The Fisher Information Matrix for a non-linear least squares batch filter with zero mean Gaussian measurement uncertainty is given by the inverse of the covariance matrix calculated with true values for the uncertain parameters⁶. In this case that implies that the errors are all zero, and that the INS estimates are the true values. The covariance matrix is defined in Equation (4.5), where H^n is the stacked matrix of partial derivatives of each measurement equation with respect to each unknown parameter, and is given in Equation (4.6). R_n is the stacked uncertainty values for each measurement, and is given in Equation (4.7).

$$P \equiv J^{-1} = (H^{nT} R_n^{-1} H^n)^{-1} \tag{4.5}$$

$$H^n = \begin{bmatrix} \frac{\partial h_R(\underline{x}_{INS}(1), \underline{v}_{INS}(1), \underline{x}, t_{f_image})}{\partial \underline{x}} \\ \frac{\partial h_{\dot{R}}(\underline{x}_{INS}(1), \underline{v}_{INS}(1), \underline{x}, t_{f_image})}{\partial \underline{x}} \\ \vdots \\ \frac{\partial h_R(\underline{x}_{INS}(n_image), \underline{v}_{INS}(n_image), \underline{x}, 0)}{\partial \underline{x}} \\ \frac{\partial h_{\dot{R}}(\underline{x}_{INS}(n_image), \underline{v}_{INS}(n_image), \underline{x}, 0)}{\partial \underline{x}} \end{bmatrix}_{\underline{x}=\underline{x}_{TRUE}} \tag{4.6}$$

$$R_n = \text{diag}([\sigma_R^2(1) \ \sigma_R^2(1) \ \dots \ \sigma_R^2(n_image) \ \sigma_R^2(n_image)]) \tag{4.7}$$

To quantify the magnitude of the uncertainty region from the covariance matrix we can consider the probability that the true values lie within the hyperellipsoid given by Equation (4.8).

$$(\underline{x} - \hat{\underline{x}})^T P^{-1} (\underline{x} - \hat{\underline{x}}) = l^2 \tag{4.8}$$

The semi-axis lengths of this hyperellipsoid are defined by the square roots of the eigenvalues of the covariance matrix scaled by l . For this paper, only the 3x3 subset of the covariance matrix that relates to the position estimates is considered. From Bryson⁵, for a 3x3 covariance matrix the probability region for a given ellipsoid is given in Equation (4.9). For a value of $l=1$ this relates to a probability region of 20%, and a value of $l=2$ relates to a probability region of 74%.

$$\text{Pr} = \text{erf}\left(\frac{l}{\sqrt{2}}\right) - \sqrt{\frac{2}{\pi}} l e^{(-1/2l^2)} \tag{4.9}$$

The cost on the accuracy of the position estimates is proposed to be the sum of the squares of the ellipsoid semi-axes (x_r, y_r, z_r) defined by the eigenvalues of the covariance matrix.

5. Trajectory optimization

A direct optimization approach was taken which is based on a finite-dimensional discretization of the original control problem. This step reduces the problem to that of a finite-dimensional constrained optimization problem that can be solved using the Sequential Quadratic Programming (SQP) solvers available in the MathWorks Optimization Toolbox⁹. The benefit of using a direct optimization approach, over the variational approach as described in Bryson⁵, is the ease with which the problem can be posed, and the relaxed requirements on the initial guess for the solution.

A fixed flight time was chosen, and the parameters to be determined are the sequence of piecewise constant acceleration demands over equidistant time intervals (Figure 3). In addition to determining the time varying controls, the thrust level, and the initial cross range offset are set as parameters to be determined.

For a given sequence of demands the dynamic states are calculated by numerically integrating the state equations. The scalar cost function, and the vector inequality constraint functions, are then evaluated and

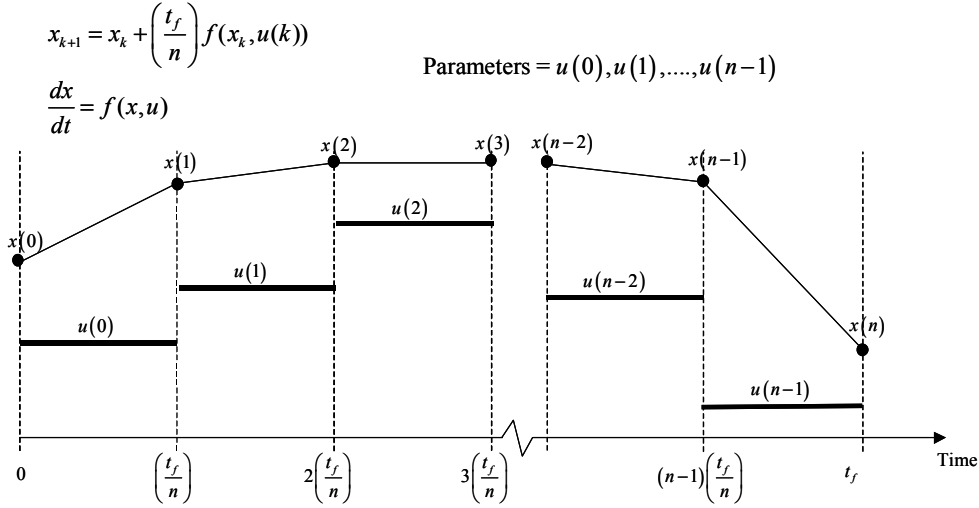


Figure 3: Discretization of Control Problem

passed to the optimization routines. The cost function for this paper is made up of the components given in Equation (5.1).

$$J_{Tot} = \frac{J_{cr}}{\alpha_{cr}} + \frac{J_p}{\alpha_p} + \frac{J_{control}}{\alpha_{control}} + \underline{G}_{Term}^T \underline{G}_{Term}$$

$$J_{cr} = \text{Cost on the dwell time}$$

$$J_p = \text{Cost on the CRLB} \quad (5.1)$$

$$J_{control} = \text{Cost on the acceleration demands}$$

$$\underline{G}_{Term} = \text{Terminal constraints}$$

$$\alpha_{cr}, \alpha_p, \alpha_{control} = \text{Weighting values.}$$

The cost on the dwell time to achieve a desired cross range resolution is given in Equation (5.2), where t_f is the time of flight, and n is the number of discrete intervals that the flight is divided into. $W_{cr}(R)$ is a function which weights the cost during the period where imaging can take place (Figure 4). The last three nodes are not included in the cost function to represent the transition from imaging, to achieving the desired angle of attack at impact.

$$J_{cr} = \left(\frac{t_f}{n}\right) \sum_{k=1}^{n-3} \left(\left(\frac{crDT(k)}{cr} \right)^2 W_{cr}(R(k)) \right) \quad (5.2)$$

The cost on the uncertainty associated with the estimates of the target location is given in Equation (5.3), where x_r, y_r, z_r are the eigenvalues of the subset of the covariance matrix in (4.6) associated with the position error estimates. It is assumed that measurements are taken at each node in the trajectory when the conditions are satisfactory, and that the dwell time is chosen to obtain a cross range resolution of cr .

$$J_p = (x_r^2 + y_r^2 + z_r^2) \quad (5.3)$$

The cost on the acceleration demands is given in Equation (5.4), where the aim is to smooth the demands over the time of flight.

$$J_{control} = \left(\frac{t_f}{n}\right) \sum_{k=0}^{n-1} \left((a_z(k) - a_z(k-1))^2 + (a_y(k) - a_y(k-1))^2 \right)$$

$$a_z(-1) = 1, \quad a_y(-1) = 0. \quad (5.4)$$

The constraints at the final flight time are given in Equation (5.5), and are incorporated by augmenting the cost function in (5.1). There are six constraints, including the cross range distance, height, speed, angles of approach, and total angle of attack. There is no constraint on the final downrange location since the optimization runs with a fixed flight time. For the purposes of calculating the dwell time and the CRLB it is always assumed that the target is located where the trajectory terminates.

$$\underline{G}_{Term} = \begin{bmatrix} \left(\frac{y(n)}{100} \right) \\ \left(\frac{h(n)}{100} \right) \\ \left(\frac{V_{Term} - V(n)}{10} \right) \\ \left(\frac{\gamma_{Term} - \gamma(n)}{(5\pi/180)} \right) \\ \left(\frac{\psi_{Term} - \psi(n)}{(5\pi/180)} \right) \\ \left(\frac{\alpha(n)}{(5\pi/180)} \right) \end{bmatrix} \quad (5.5)$$

In addition to minimizing the cost function, at each node the resulting trajectory has to satisfy a number of interior point constraints on the states. The three inequality constraints are: -

- i) $|\alpha| \leq \alpha_{max}$
- ii) $|\sigma_v| \leq \sigma_{v_max} \quad (R < R_{Acquire})$
- iii) $|\psi_{DBS}| \geq 5^\circ \quad (R < R_{Acquire} \ \& \ k < n-2)$

6. Example optimal trajectory results

Two resulting optimal trajectories are shown in Figures 5 and 6, where the requirements are specified in Table 3. The first trajectory has no cost on the expected

uncertainty on the position error estimates. The aim is therefore purely to achieve high-resolution images with minimal dwell time during the engagement. The trajectory is seen to initially pull away from the target in order to achieve the desired angular offset between the line of sight and the velocity vector. The extent of the maneuver is only limited by the look angle constraint. As the range to go reduces, the angular offset is maintained by increasing the acceleration demands, until they are forced to reduce to satisfy the angle of attack constraint at impact. Since the thrust level is the maximum value, the acceleration demands have to be lower than their maximum values due to induced drag causing the velocity to drop below the constraint set at impact. For this trajectory the ellipsoid derived from the covariance matrix is shown in Figure 7. The shape of the uncertainty region shows that from the sequence of generated images the estimate of the downrange target location is very poor, and would likely result in large miss distances being achieved.

The second trajectory shown in Figure 6 now introduces the cost on the position estimate uncertainty, and the uncertainty ellipsoid is shown in Figure 8. The shape of the trajectory clearly provides the batch filter with more information from which the target location can be estimated. This reduced uncertainty region is achieved by allowing the dwell time to increase, and effectively “sweeping” the target in yaw to achieve better downrange position estimates.

It is difficult to infer from these results a general strategy for a guidance law using a DBS seeker, since these results are for a specific airframe, and for a single set of weights on the cost function. They do though demonstrate the high degree of coupling between the capabilities of the airframe, and the expected accuracy to which the seeker and the guidance filters can estimate the target location. This is due to the increasing acceleration demands as the target is approached. Not only does the airframe require the capability to achieve these high demands, the thrust capabilities have to be sufficient to maintain the velocity if the warhead is to be effective at impact.

7. A trajectory following guidance law

A proposed guidance law designed to achieve small miss distances, and which shapes the trajectory to follow the nominal optimal trajectories is given in Equation (7.1). The form of the guidance law is taken from Zipfel², and is a modified form of velocity pursuit with the output an acceleration demand vector in earth axes. The first cross product term generates acceleration demands that drive the velocity vector (\vec{u}_v) to lie along the line of sight (\vec{u}_{LOS}), hence assuring small miss distances. The second cross product term bends the trajectory toward a desired Line Of Approach (LOA). The bias gain (G) defines the shape of the trajectory followed.

$$\vec{a}_{zd}^e = KV((\vec{u}_v \times \vec{u}_{LOS}) \times \vec{u}_v - G(R)((\vec{u}_v \times \vec{u}_{LOA}(R)) \times \vec{u}_v)) \quad (7.1)$$

To match the acceleration demands from the open loop trajectories, both the line of approach, and the bias gain can be made functions of the range to go. Since the open loop trajectories are constrained to a yaw flightpath angle of -90 degrees at impact, the line of approach can be defined by a single pitch attitude angle θ_{LOA} in Equation (7.2).

$$\vec{u}_{LOA} = - \begin{bmatrix} 0 \\ \cos(\theta_{LOA}(R)) \\ \sin(\theta_{LOA}(R)) \end{bmatrix} \quad (7.2)$$

The bias gain, and the line of approach attitude, can be derived from the open loop trajectories using both Equation (7.1), and the transformation of the acceleration demands in velocity axes to earth axes in Equation (7.3). In Equation (7.3) $T_{v \rightarrow e}$ is the transformation matrix given in Equation (7.4).

$$\vec{a}_{zd}^e = T_{v \rightarrow e} \begin{bmatrix} 0 \\ a_y \\ a_z \end{bmatrix}_{\text{Optimal}} \quad (7.3)$$

$$T_{v \rightarrow e} = \begin{bmatrix} \cos \gamma \cos \psi & -\sin \psi & -\sin \gamma \cos \psi \\ \cos \gamma \sin \psi & \cos \psi & -\sin \gamma \sin \psi \\ \sin \gamma & 0 & \cos \gamma \end{bmatrix} \quad (7.4)$$

The resulting analytical expressions for $G(R)$ and $\theta_{LOA}(R)$ are not trivial, and are not included in this paper. An example of the resulting gain values derived from the optimal trajectory found in the previous section is shown in Figure 9.

The closed loop performance of the guidance law is demonstrated using the Simulink^{®10} model in Figure 10. The model implements the point mass dynamics in Equation (2.1), and assumes a simple first order response for the autopilot dynamics. The resulting closed loop trajectory is shown along with the nominal open loop values in Figure 11. The match is clearly very close, and the guidance law has successfully been demonstrated in more detailed 6DoF models, and in the presence of uncertain target locations and INS errors.

8. Conclusions

This paper has demonstrated that optimal trajectories can successfully be generated to achieve both the image quality required to identify a target during the terminal stages of an engagement, and also the requirements for the guidance filters to estimate the target location within acceptable bounds to achieve low miss distances.

9. Acknowledgements

This work has been funded by UK MOD.

10. References

- [1] S.A.Hovanesian, "Introduction to Synthetic Array and Imaging Radars", *Artech House*, 1980.
- [2] Peter H. Zipfel, "Squint Angle Guidance for Missiles with SAR Sensors", *AIAA Missile Sciences Conference*, 3-5 December 1996.
- [3] Renjith R. Kumar, Hans Seywald, "Three-Dimensional Air-to-Air Missile Trajectory Shaping", *Journal of Guidance, Control, and Dynamics*, Vol. 18, No. 3, May-June 1995.
- [4] Branko Ristic, Sanjeev Arulampalam, James McCarthy, "Target Motion Analysis Using Range-only Measurements: Algorithms, Performance and Application to ISAR Data", *Signal Processing*.
- [5] Arthur E. Bryson, Yu-Chi Ho, "Applied Optimal Control", *Taylor and Francis*.
- [6] Yaakov Bar-Shalom, X. Rong Li, Thiagalingam Kirubarajan, "Estimation with Applications to Tracking and Navigation: Theory Algorithms and Software", *John Wiley & Sons*, 2001.
- [7] Asif Farooq, David Limbeer, "Trajectory Optimization for Air-to-Surface Missiles with Imaging Radars", *Journal of Guidance, Control, and Dynamics*, Vol. 25, No.5, September-October 2002.
- [8] M. Rollason, D. Salmond and M. Evans, "Parameter Estimation for Terminal Guidance Using a Doppler Beam Sharpening Radar", *AIAA Guidance, Navigation, and Control Conference, August 2003*, AIAA-2003-5447.
- [9] The MathWorks Inc, "Optimization Toolbox User's Guide Version 2.2", July 2002.
- [10] The MathWorks Inc, "Simulink Reference Version 5", July 2002.

Parameter	Description	Value	Units
m	Mass	500	kg
S_{Ref}	Reference area	$\frac{\pi}{4}0.41^2$	m^2
T	Thrust level	1000 to 2500	N
C_{D0}	Drag coefficient	0.3	-
k	Induced drag coefficient	0.03	-
ρ_0	Air density at sea level	1.225	kg/m^3
T_0	Temperature at sea level	288.16	K
L	Lapse rate	-0.0065	K/m
R	Gas constant	287.26	J/kg/K
$C_{L\alpha}$	Lift coefficient derivative w.r.t. α .	50	-

Table 1: Missile Dynamic Model Configuration

Parameter	Description	Value	Units
λ	Radar wavelength	$\frac{3 \times 10^8}{(35GHz)}$	m
c_r	Desired cross range resolution	3	m
R_{Res}	Range resolution	1	m
$R_{Acquire}$	Acquisition range	5000	m
σ_{v_Max}	Maximum look angle	40	deg

Table 2: DBS Characteristics

Parameter	Description	Value	Units
$V(0)$	Initial velocity	270	m/s
$h(0)$	Initial height	1000	m
$\gamma(0), \psi(0)$	Initial flightpath angles	0	deg
V_{Term}	Velocity at impact	270	m/s
$\gamma_{Term} \psi_{Term}$	Pitch and yaw flightpath angles at impact	[-60,-90]	deg
α_{max}	Maximum angle of attack	10	deg
t_f	Time of flight	32	sec
n	Number of nodes	55	-

Table 3: Optimization Criteria

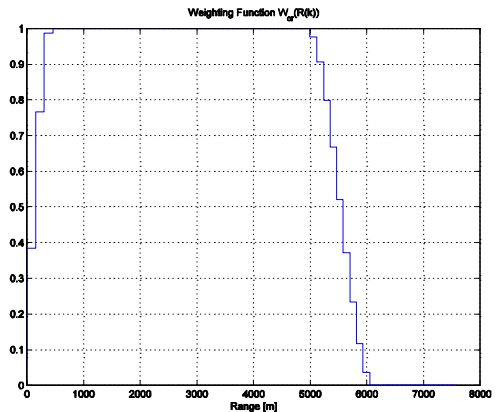


Figure 4: Weighting Function

Start Range = 7555.9654, Gimbal Limit = 40, Acquisition Range = 5000, Flight Time = 32
 Thrust = 2500, $V_0 = 270$, Max height = 1054.383, Max cross range distance = 1837.4066
 Velocity at impact = 269.9835, Flightpath angle at impact = -59.9717

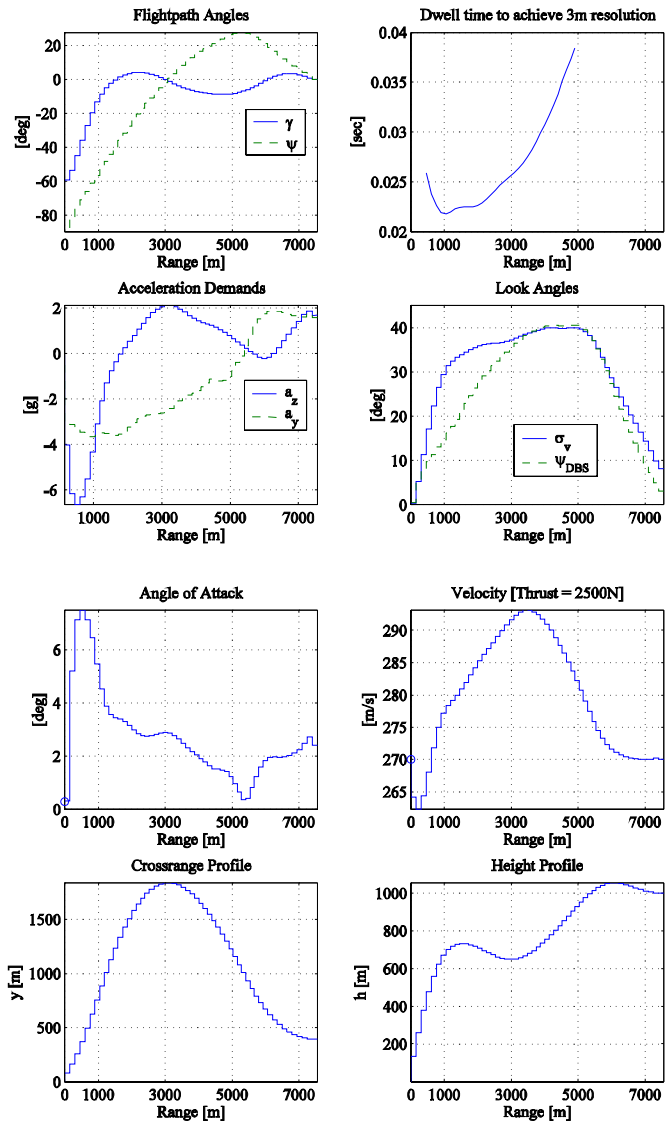
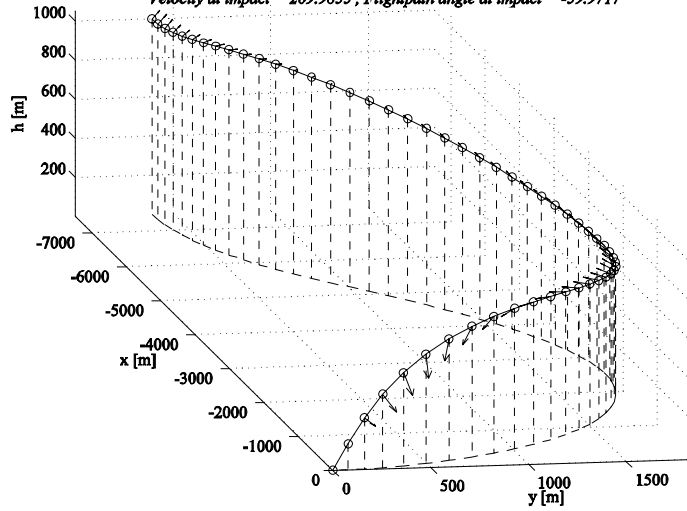


Figure 5: Optimal trajectory with the cost only on the dwell time

Start Range = 7480.0668, Gimbal Limit = 40, Acquisition Range = 5000, Flight Time = 32
 Thrust = 2500, $V_0 = 270$, Max height = 1357.5236, Max cross range distance = 2357.5995
 Velocity at impact = 269.963, Flightpath angle at impact = -59.9978

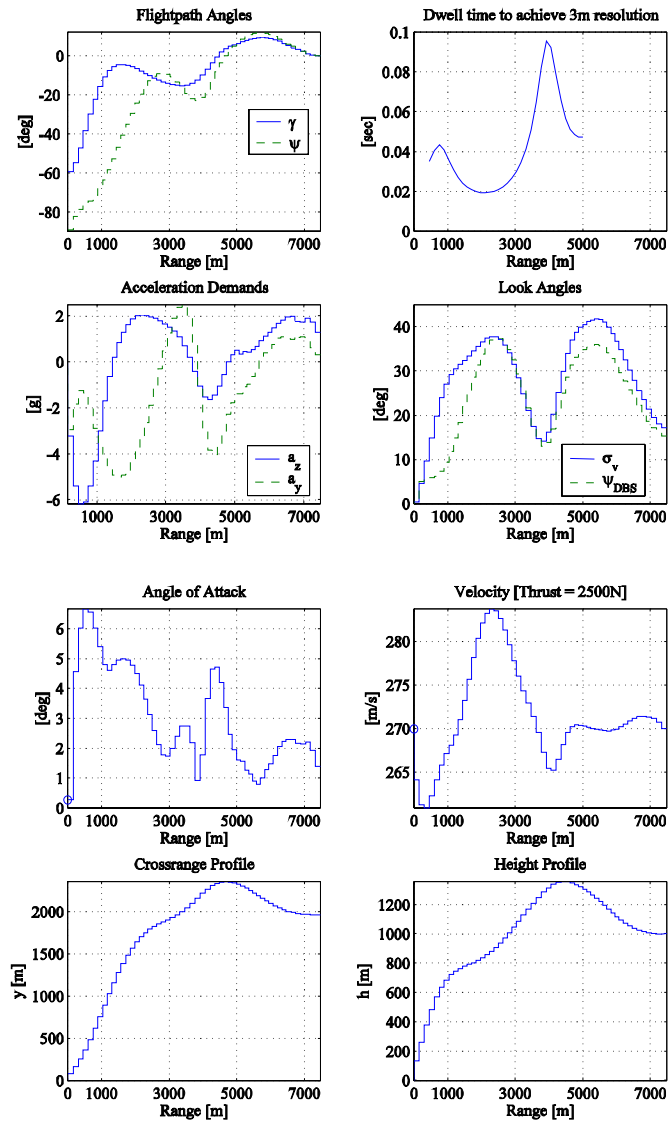
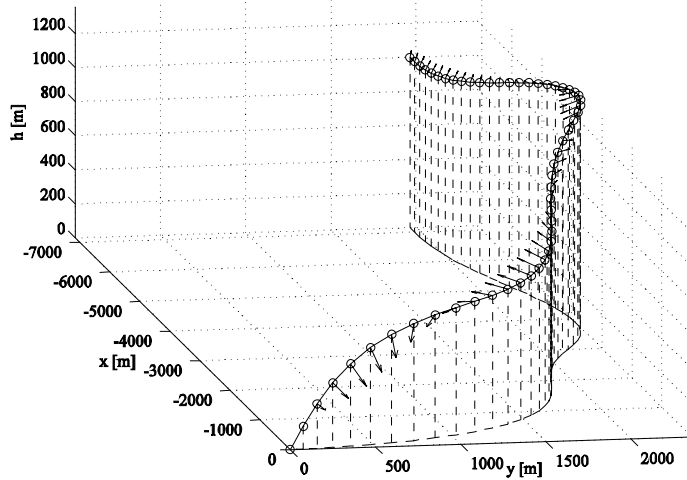


Figure 6: Optimal trajectory with cost on the CRLB

Cramer Rao Lower Bound, Dive Angle = 60deg, cr = 3, Rres=1
 Probability = 73.85%, xr = 14.8425m, yr = 3.9472m, zr = 0.70757m

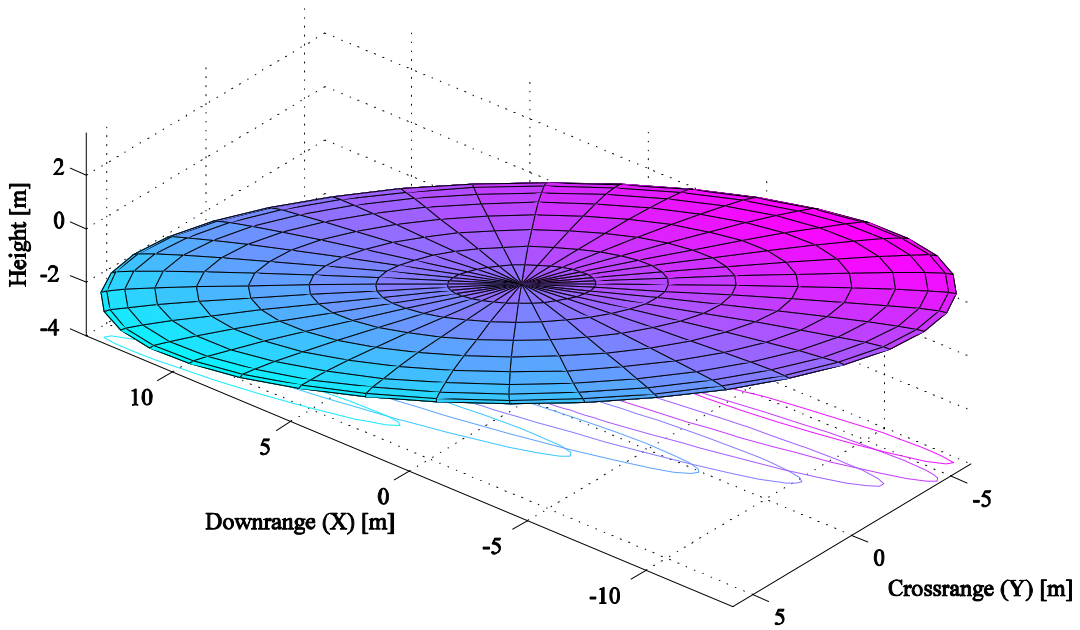


Figure 7: Position estimate uncertainty for trajectory with the cost only on the dwell time

Cramer Rao Lower Bound, Dive Angle = 60deg, cr = 3, Rres=1
 Probability = 73.85%, xr = 2.3473m, yr = 2.0214m, zr = 0.63547m

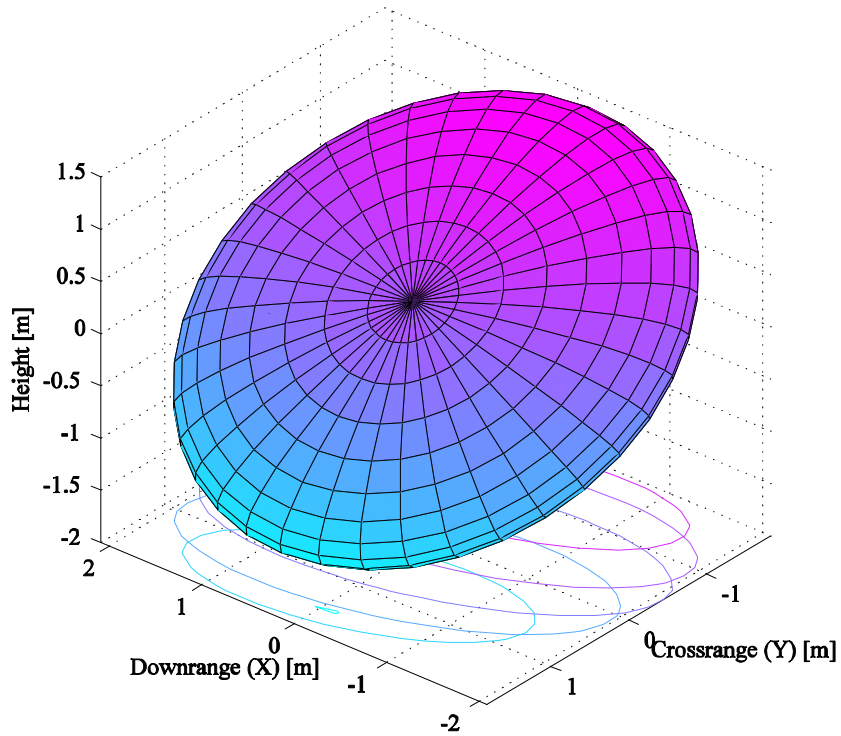


Figure 8: Position estimate uncertainty for trajectory with the cost on the CRLB

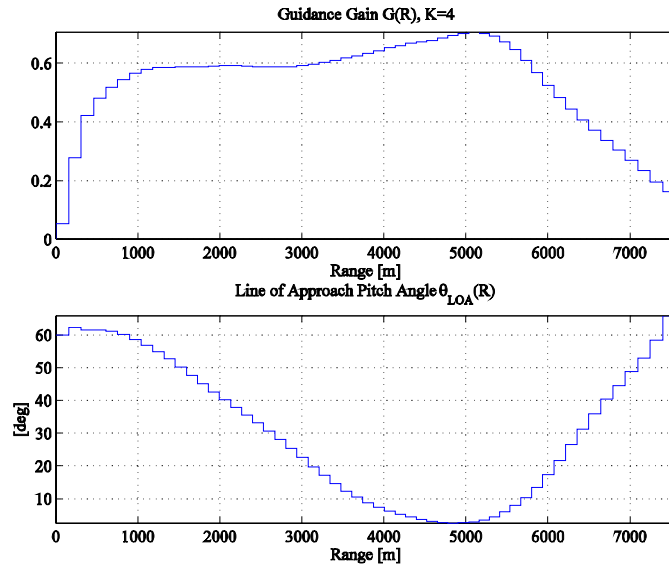


Figure 9: Gains for trajectory shaping guidance law

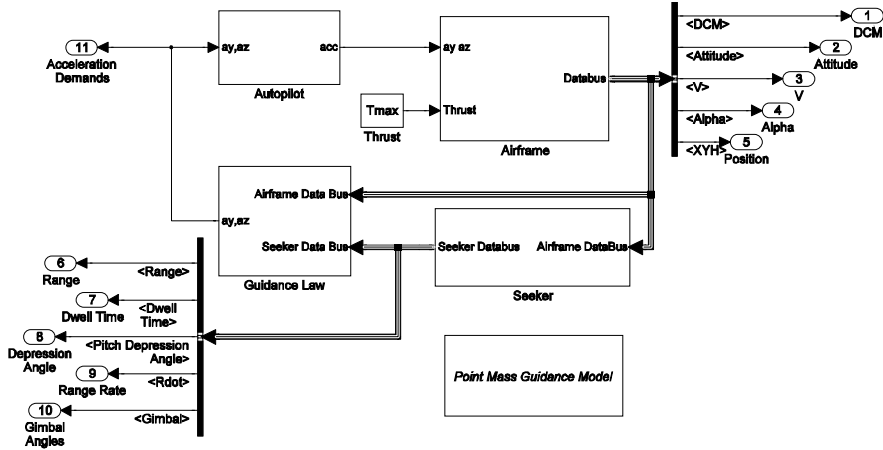


Figure 10: Closed loop guidance model

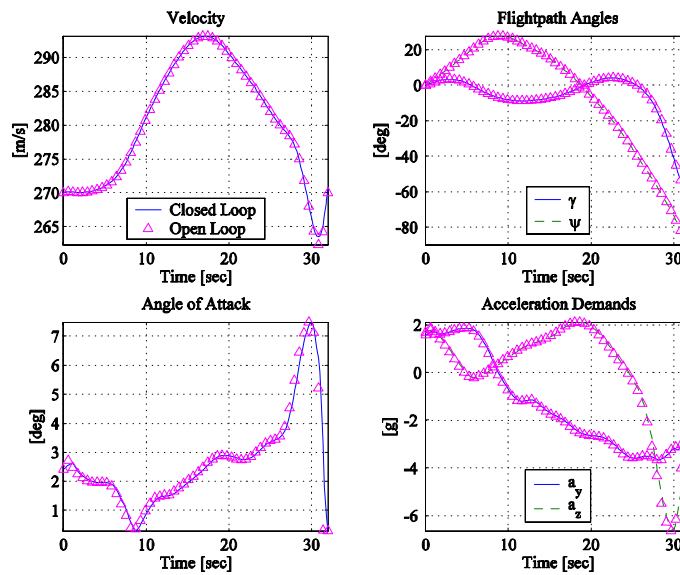


Figure 11: Comparison between open and closed loop trajectories